Chemical Papers
https://doi.org/10.1007/s11696-022-02158-4

ORIGINAL PAPER

Synthesis, theoretical and experimental spectroscopic properties, molecular docking, ADMET, and RDG analysis of copper(II) complex of dichloro(1,10-phenanthroline)(1,2,4-triazole-3-carboxcylic acid)

Sibel Celik[1] · Serdar Badoğlu[2] · Senay Yurdakul[3]

Received: 27 October 2021 / Accepted: 3 March 2022

Abstract
A new dichloro(1,10-phenanthroline)(1,2,4-triazole-3-carboxylic-acid)copper(II) was synthesized, and the most stable optimized structure was determined using the B3LYP/LANL2DZ basis set, followed by FTIR and NMR characterization. The molecular geometric structure analysis and vibrational frequencies of the Cu(II) complex were calculated by using density functional theory calculations in the ground state. Metal-ligand and intra-ligand vibrations were investigated using vibrational analysis, and the obtained computational values were compared with the experimental values. The ProTox-II webserver was utilized for toxicological evaluation of the organism and organ, as well as molecular mechanisms of toxicity evidenced by the median lethal dose (LD_{50}). SwissADME prediction was performed ADMET properties. Reduced density gradient (RDG) analysis is employed to study the weak interactions within the molecule. The nature of the chemical bonds in the $[Cu(phen)(TCA)_2Cl_2]$ complex is investigated using electron localization function (ELF) analysis. MEPs, HOMO, LUMO, global reactivity descriptors, and Fukui functions are performed to study the chemical reactivity of the compound. Molecular docking studies are performed to predict the antibacterial, antidepressant, and anti-anxiety active site of the complex. $Cu(phen)(TCA)_2Cl_2$ was defined and used to evaluate the antibacterial properties of this Cu(II) complex against *B. subtilis*.

Keywords 1,2,4-Triazole-3-carboxcylic acid · DFT · Reduced density gradient (RDG) · Electron localization function (ELF) · Molecular docking · Toxicity

Introduction

Metal complexes have received a lot of attention recently because of their potential benefits in the fields of medical applications and metal-based pharmaceutical products (Onawumi et al. 2013). In particular, among all the widely studied transition metals, copper is gaining intense attention due to its two common oxidation states (Chen et al. 2007), biological significance, and different stereo-electronic preferences of its electronic properties (Dunaj-Jurco et al. 1988; Houser et al. 1996; Malmatrom and Aasa 1993; Lappalainen and Saraste 1994; Henkel et al. 1995). Since copper complexes have a wide range of pharmacological effects, including antibacterial, antifungal, antiviral, anticancer, and anti-inflammatory activity, this has led to the investigation of copper-based drugs (Chandraleka et al. 2014). Furthermore, copper is a crucial cofactor for many proteins and enzymes that are critical for human health since it is required for proper physiological functioning and metabolic processes in living organisms, including DNA synthesis and angiogenesis (Tapiero et al. 2003).

1,2,4-Triazole-3-carboxylic acid and 1,10-phenanthroline molecules exist in the structure of the synthesized complex. Compounds of 1,2,4 triazole-3-carboxylic acid derivatives are useful in therapy, particularly for the treatment of neurological, psychiatric, pain, and gastrointestinal disorders (Yurdakul and Tanrıbuyurdu 2012). The other molecule is 1,10-phenanthroline; transition metal complexes based on 1,10-phenanthroline and its derivatives are frequently

✉ Sibel Celik
sibelcelik@ahievran.edu.tr

[1] Vocational School of Health Services, Kırşehir Ahi Evran University, Kırşehir, Turkey

[2] Faculty of Air Transportation, Department of Flight Training, University of Turkish Aeronautical Association, Ankara, Turkey

[3] Department of Physics, Faculty of Science, Gazi University, Ankara, Turkey

Published online: 20 March 2022

studied for their anticancer, catalytic, redox, photochemical, and photophysical properties (Bergamo et al. 2018; Luman and Castellano 2003; Accorsi et al. 2009; Bencini and Lippolis 2010). In coordination chemistry, there have been several experimental and theoretical investigations into the biologically important aromatic compounds (Ramakrishnan and Palaniandavar 2005; Reiher et al. 2004; Schilt and Taylor 1959; Machura et al. 2011; Robertazzi et al. 2009). Also, previous studies (Kargar et al. 2021a, b, c) are investigating DNA-binding studies and DFT calculations of synthesized N,O-bidentate Schiff base ligands and their Zn and Cu complexes. Studies of Kargar et al. are such published works in which N,O-bidentate Schiff base ligands and their Zn and Cu complexes are synthesized, and their structures, spectroscopic properties, antibacterial activities, molecular docking, and DNA-binding investigations are reported.list. So, we have

The aim of this study is to calculate and experimentally investigate the synthesis, characterization and DFT of the new copper(II) complex, dichloro(1,10-phenanthroline)(1,2,4-triazole-3-carboxylicacid)copper(II), consisting of two independent mononuclear molecules. To understand the stability of a compound, the intramolecular weak interactions were performed via reduced density gradient (RDG) and electron localizing function (ELF). The chemical reactivity of the synthesized complex was determined using molecular reactivity descriptors such as condensed Fukui functions, HOMO–LUMO analysis, NBO, and MEP analyses. Finally, the copper(II) complex was also molecular docked to the active sites of mitochondrial outer membrane-anchored monoamine oxidase (MAO) and Bacillus subtilis receptor proteins in order to determine their binding method. The toxicity of metallo-drugs is problematic, so the organ toxicities and ADMET properties of the Cu(II) complex were estimated.

Experimental

Synthesis of complex

$CuCl_2{\cdot}2H_2O$ (0.5 mmol, 170.48 mg) dissolved in 5 ml distilled water and 1,2,4-triazole-3-carboxylic acid (0.5 mmol, 113.07 mg) dissolved in 15 ml distilled water were added together while stirring at 323°K. The resulting blue solution was allowed to react for 30 min, and 1,10-phenanthroline (0.5 mmol, 99.1 mg) dissolved in ethanol (5 ml) was added. Light blue color compound was obtained by slow evaporation over a period of one month (yield 55%). [Cu(C12H8N2)Cl_2(C3H3N3O2)$_2$], [C18H16Cl2CuN8O4], CHN Theoretical: C: 39.98%, H: 2.61%, N: 20.72%. Experimental: C: 41.51%, H: 2.94%, N: 20.01%.

Instrumentation for recording spectra

The infrared spectrum of [Cu(phen)$(TCA)_2Cl_2$] complex was recorded between 4000 and 550 cm^{-1} on the Bruker Vertex 80 FTIR spectrometer. Far-IR spectra were recorded between 700 and 100 cm^{-1} on Bruker IFS 66/S system. ^1H NMR spectrum of the title compound was recorded on a 300 MHz Bruker Avance FT-NMR spectrometer, and the solvent was D_2O.

Computational methods

Computational details

The DFT calculations were performed using GAUSSIAN09 (Frisch et al. 2009). The DFT-B3LYP approach with the LANL2DZ basis set is used to optimize the geometry of the [Cu(phen)$(TCA)_2Cl_2$] complex. The optimized molecular structure is used to perform vibrational frequencies, HOMO–LUMO orbitals, global chemical reactivity parameters, Fukui functions, NBO, and MEP analysis of the studied compound. HOMO, LUMO, and MEP analysis were visualized using GaussView 5.0 (Dennington et al. 2009). NMR calculations were carried out at B3LYP/LANL2DZ level with GIAO/PCM approach, and the solvent was water. Chemical shifts were derived with respect to the isotropic shieldings of the TMS (tetramethylsilane). By employing Multiwfn (Lu and Chen 2012) and the molecular visualization program VMD (Humphrey et al. 1996), RDG analysis leads to an easy-to-catch pictorial visualization of various kinds of non-covalent interactions directly in real space. ADME properties of the Cu(II) complex are obtained using Pre-ADMET software (https://www.preadmet.com) and SwissADME tool (https://www.swissadme.ch/index.php.). The ProTox-II webserver (http://tox.charite.de/protox_II/) was used to estimate the organ toxicities and toxicological end points of the title complex and their LD50.

Molecular docking procedure

The molecular docking of the chemical compounds–proteins binding site was performed using AutoDock 2.2.6 software (Morris et al. 1998). The docked complexes were visualized using PYMOL (DeLano 2002) and Discover Studio software (https://www.3ds.com/ products-services/biovia/products/molecular-modelingsimulation/biovia-discovery-studio/visualization/). The three-dimensional structure of PDB (PDB ID: 2Z5X, 3EU4) was obtained from the RSCB protein data bank (https://www.rcsb.org). The 2Z5X and 3EU4 proteins were simulated using the open-source server PROCHECK, and the Ramachandran plot for the proteins was examined.

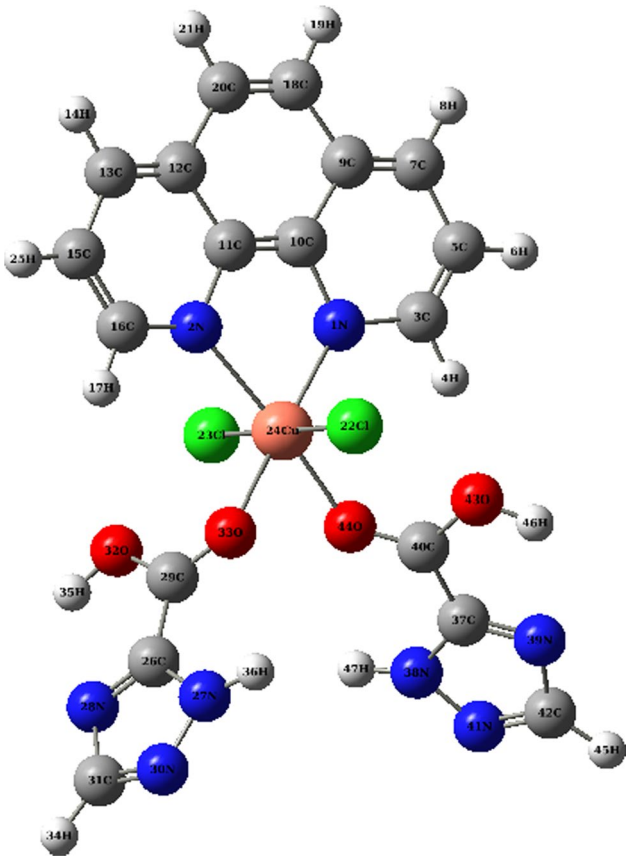

Fig. 1 Molecular structure of $[Cu(phen)(TCA)_2Cl_2]$

Results and discussion

Geometrical parameters of complex

The optimized molecular structure and atomic numbering of the Cu(II) complex are shown in Fig. 1. The $[Cu(phen)(TCA)_2Cl_2]$ geometry was optimized using the DFT/B3LYP method with LANL2DZ basis set. The calculated stabilization energy of copper(II) complex was $E = -3563.045417$ a.u. The newly synthesized Cu(II) complex is composed of one Cu(II) ion, one 1,2,4 triazole-3-carboxylic acid (TCA) and 1,10-phenanthroline (phen) molecule, and two Cl anions (Fig. 1). Because the synthesized complex lacked X-ray data, the work of Zhu (Zhu et al. 2008), which has a comparable structure, was used as a reference. Optimized geometric parameters are presented in Table 1 (in Supplementary Information S1) and compared to X-ray crystallographic data of the [chlorido (1,10-phenanthroline) (1H-1,2,4-triazole-3-carboxylato) copper (II)] complex reported by Zhu et al. The calculated geometrical parameters are in good agreement with the reference values. For instance, experimental and predicted Cu–N length and N–Cu–N angle (phen N5 and N6 atoms) values are highly consistent. These values agree with those reported in the literature (Hammuda et al. 2020), indicating that phenanthroline has good coordination ability. The DFT calculations demonstrate that the metal–oxygen bond length is slightly shorter than the metal–nitrogen bond length [Cu–O: 1.99 Å, Cu–N: 2.12 Å]. The Cu–Cl distance in this compound was calculated to be 2.42 Å, suggesting that the chlorine atoms are loosely bonded. Also, the

Table 1 Selected optimized geometrical parameters of $[Cu(phen)(TCA)_2Cl_2]$ obtained by B3LYP/LANL2DZ basis set

Parameters	Bond lengths (Å)		Parameters	Bond angles (°)		Parameters	Bond angles (°)	
	Calc	XRD*		Calc	XRD*		Calc	XRD*
$\Gamma(Cu_1–N_5)$	1.9984	2.026	$\angle(N_5–Cu_1–N_6)$	81.40	81.67	$\angle(Cu_1–N_6–C_{26})$	130.10	129.7
$\Gamma(Cu_1–N_6)$	2.1205	2.007	$\angle(N_5–Cu_1–O_7)$	57.36		$\angle(C_{20}–N_6–C_{26})$	119.59	
$\Gamma(Cu_1–O_7)$	4.9165		$\angle(N_5–Cu_1–O_{34})$	168.43	166.89	$\angle(Cu_1–O_7–C_9)$	122.22	
$\Gamma(Cu_1–O_{34})$	2.0574		$\angle(N_5–Cu_1–Cl_{46})$	92.61		$\angle(N_5–C_{19}–C_{20})$	117.42	116.1
$\Gamma(Cu_1–Cl_{46})$	2.4286	2.4443	$\angle(N_5–Cu_1–Cl_{47})$	94.09	104.68	$\angle(C_{18}–C_{19}–C_{20})$	120.32	120.8
$\Gamma(Cu_1–Cl_{47})$	2.4063		$\angle(N_6–Cu_1–O_7)$	138.52		$\angle(N_6–C_{20}–C_{19})$	116.87	116.7
$\Gamma(N_2–N_3)$	1.3777		$\angle(N_6–Cu_1–O_{34})$	87.88	89.02	$\angle(N_6–C_{20}–C_{21})$	122.84	123.7
$\Gamma(N_2–C_{11})$	1.3586		$\angle(N_6–Cu_1–Cl_{46})$	114.87		$\angle(C_{19}–C_{20}–C_{21})$	120.28	119.7
$\Gamma(N_3–C_{10})$	1.3642		$\angle(N_6–Cu_1–Cl_{47})$	129.71	94.25	$\angle(C_{20}–C_{21}–C_{22})$	116.87	117.1
$\Gamma(N_4–H_{43})$	1.0367		$\angle(O_7–Cu_1–O_{34})$	132.74		$\angle(C_{20}–C_{21}–C_{30})$	118.65	118.9
$\Gamma(N_4–C_{10})$	1.3559		$\angle(O_7–Cu_1–Cl_{46})$	74.68		$\angle(Cu_1–N_5–C_{19})$	113.86	112.3
$\Gamma(N_5–C_{12})$	1.3406	1.323	$\angle(O_{34}–Cu_1–Cl_{46})$	95.86	97.04	$\angle(C_{12}–N_5–C_{19})$	120.34	118.3
$\Gamma(N_5–C_{19})$	1.3702	1.363	$\angle(O_{34}–Cu_1–Cl_{47})$	89.38		$\angle(Cu_1–N_6–C_{20})$	110.24	112.8
$\Gamma(N_6–C_{20})$	1.3696	1.359	$\angle(Cl_{46}–Cu_1–Cl_{47})$	115.35		$\angle(Cu_1–O_{34}–C_{35})$	135.76	
$\Gamma(C_{12}–C_{14})$	1.4209	1.396	$\angle(Cu_1–N_5–C_{12})$	125.73	129.2	$\angle(C_{18}–C_{28}–H_{29})$	118.44	

*X-Ray data taken from Zhu et al. (2008)

N_5–Cu–Cl_{46} and O_{34}–Cu–Cl_{46} planes are calculated at an angle of about 90°, which is virtually perpendicular.

Vibrational assignments

The vibrational wavenumbers, calculated IR intensities, and approximate assignments of those normal modes of [Cu(phen)$(TCA)_2Cl_2$] complex are given in Table S2 together with the vibrational frequencies of free phen and free TCA ligands. The experimental mid-IR and far-IR spectra are given in Fig. 2. The first detailed vibrational assignment for the free 1,2,4-triazole-3-carboxylic acid molecule was made in our previous study (Yurdakul and Tanrıbuyurdu 2012), and calculated and experimental frequencies are reported there. The experimental and theoretical FTIR spectra of [Cu(phen)$(TCA)_2Cl_2$] suggest that the vibrations also contribute to the geometrical results. The weak bands at 3360 and 3392 cm^{-1} in the experimental spectrum are assigned to the OH stretching vibrations of the carboxyl group. Based on IR spectra, the C–H stretching vibrations of both species have been characterized. For TCA, this mode generates a very strong intensity band at

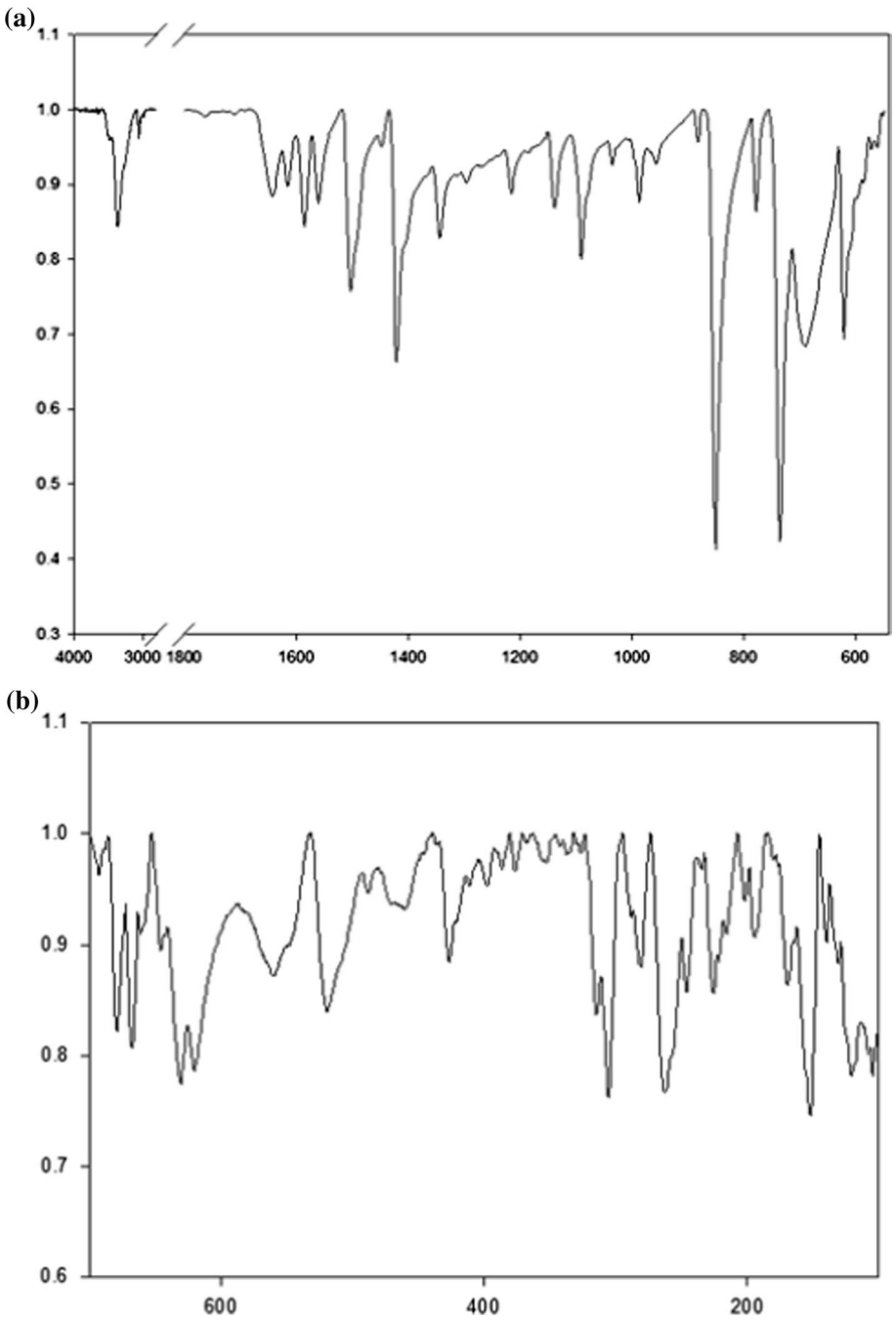

Fig. 2 Experimental (**a**) mid-IR and (**b**) far IR of [Cu(phen)$(TCA)_2Cl_2$]

3112 cm^{-1}. Upon complexation, this vibration is shifted to a lower energy by 10 cm^{-1}. Similarly, the carbonyl (C=O) stretching vibration shifted from 1734 cm^{-1} (very strong) to 1724 cm^{-1} (strong). In the experimental spectra of the synthesized compound, the appearance of new bands in the 2786 cm^{-1} and 2889 cm^{-1} can be attributed to aromatic C–H symmetric stretching bands. In our calculations, these bands were predicted at 3076 and 3086 cm^{-1}. The infrared spectrum reveals absorption bands of C=C and C=N stretching vibrations characteristic of phenanthroline ligands are observed between 1344 and 1586 cm^{-1} and predicted between 1348 and 1583 cm^{-1}. While the phen and triazole ring deformations had strong peaks of 738 cm^{-1} and 1234 cm^{-1}, respectively, they were observed as weak vibrations by forming complexes with Cu(II). The bands at 811, 766, 519, and 564 cm^{-1} remain virtually unaffected by complexing. The $\nu(C–N_{triazole\ ring})$ band at 1356 cm^{-1} shown in the TCA ligand spectra shifts to 1349 cm^{-1} in the complex spectra.

Below 500 cm^{-1}, the frequency range is particularly intriguing because it can offer information on metal–ligand vibrations. The presence of new bands in the spectra of complexes occurring in this region (500–100 cm^{-1}) also shows supporting evidence of bonding, which are characteristic bands of υ(M–N) and υ(M–O) stretching vibrations, that are not observed in the phen and TCA ligand spectrum. The Cu–O stretching vibrations have been attributed to the bands located at 314 (weak), 151 (strong), and 139 (weak) cm^{-1}. These vibrations are in very good agreement with the theoretical calculations, and the TED distribution also supports this. The experimental symmetric Cu–N stretching mode in the Cu(II) complex is found at 411, 280, 215, and 168 cm^{-1}, which agrees with DFT calculations. The symmetric Cu–Cl stretching vibrations have been assigned to the medium strong band observed at 225 cm^{-1}, which is slightly higher than the calculated 233 cm^{-1}, according to the 66% TED.

Thus, the IR spectra showed that the Cu(II) ion was located at the center of the complex and bound to the nitrogen atoms of phen and oxygen of the carboxylic group.

^{1}H spectra of [Cu(phen)(TCA)$_2$Cl$_2$]

To the best of our knowledge, the presented ^{1}H NMR data are new for this title compound. The experimental ^{1}H NMR spectrum is shown in Figure S1. Heavy water (D_2O) was the solvent used in the experiment. Table S3 shows chemical shifts obtained from B3LYP/LANL2DZ level GIAO/PCM calculations by employing PCM method (solvent is water) together with the experimental data. Calculated chemical shifts correlate well with the experimental data. The linear correlation between theoretical and experimental data has been determined. The squared correlation factor (R^2) is 0.9512. A better correlation for proton shifts was not expected since the protons are located on the periphery of the molecule and are supposed to be more susceptible to solute–solvent effects (Osmialowski et al. 2001). Our theoretical calculations predicted ten signals in the theoretical spectrum. The theoretical spectrum shows ten signals, as given in Table S3. On the other hand, we have observed eight signals in the experimental spectrum. These are namely 7.0, 7.2, 7.4, 7.7, 8.4, 8.9, 9.7, and 15.1 ppm. With the help of computations, we can express that the last one arises from the carboxylic protons and it shows a shift to higher ppm which is a strong sign of intermolecular hydrogen-bonding interactions between carboxylic protons and phenanthroline. Yet it is known that the hydrogen-bonding interactions shift the resonance signals of related protons to higher frequencies (Balci 2005). The signals between 7.0 and 9.7 ppm are due to aromatic protons. They are measured mostly as multiplets due to neighbor protons in the structure, i.e., aromatic protons of phenanthroline.

NBO analysis

The inter- and intra-molecular H-bonding interactions between a wide range of chemical systems are characterized by natural bonding orbital (NBO) analysis (Pophristic et al. 1997; Pophristic 2005). To illustrate the existence of the relationships (donor–acceptor) between ligand and metal, the NBO basis was determined as a second-order perturbation theory analysis of the Fock matrix. This was done to delocalize the electron between the ligand and the metal (Liu et al. 2005;Weinhold 2005). NBO includes information such as donor (i), type, acceptor (j), occupancy, $E^{(2)}$, $\varepsilon(j) - \varepsilon(i)^b$, and $F(i, j)^c$ that $E^{(2)}$ is calculated by the equation:

$$E^{(2)} = \Delta Eij = q_i\left(F^2_{\frac{i,j}{\varepsilon_{j-\varepsilon_i}}}\right)\frac{F^2_{(ij)}}{\varepsilon_j - \varepsilon_i}.s$$

The value of the donor orbital is q_i, the diagonal elements are ε_i and ε_j, and the off-diagonal NBO Fock matrix element is $F_{(i,j)}$. Whatever the value of $E^{(2)}$ is, it means that the atoms are interacting further.

The complex's donor–acceptor interactions, bonding form, electron density, and stabilization energy were determined using the DFT/B3LYP method with LANL2DZ basis set, with the most significant donor–acceptor interaction values described in Supplementary Table S4. This table is established by the NBO analysis, and the highest stabilization energy containing $\sigma^*(Cu–N_5) \rightarrow \eta^*(Cu)$, $\eta(C_{21}) \rightarrow \sigma^*(N_6–C_{20})$, $\eta^*(C_{19}) \rightarrow \sigma^*(N_6–C_{20})$ interactions clearly leads to intermolecular charge transfer process in the complex. The further energy is transferred during $\sigma^* \rightarrow \eta^*$ transformation rather than $\eta^* \rightarrow \sigma^*$ transition. In the instance of intra-molecular hydrogen bonding, significant interaction occurs in $\sigma(C_{12}–H_{13}) \rightarrow \sigma^*(N_5–C_{19})$ (4.06 kcal/mol).

The more intense the association between electron donors and electron acceptors, the more donation propensity from electron donors to electron acceptors, and the stronger the degree of conjugation of the whole system, the higher the stabilization energy ($E^{(2)}$) value (Ajayi and Shapi 2020).

Chemical reactivity analyses

Molecular electrostatic potential (MEP) and atomic charge analysis

The MEP is used to predict the relative reactivity positions of nucleophilic and electrophilic attack sites in a species. The charge distributions and charge-related features are shown using MEP diagrams (Erdogdu et al. 2019). The compound's MEP surface analysis was determined using the DFT/B3LYP/LANL2DZ method with a structure optimized, and Fig. 3 shows the electrostatic potential surface map of this compound. Different colors are used to demonstrate the electrostatic variation on the rock. The compound's potential $V(r)$ values are $5.863e^{-2}$ to $-5.863e^{-2}$. On an MEP map, the nucleophilic reactivity of a molecule, which indicates the greatest electron repulsion, is represented in red, while the electrophilic reactivity, which indicates the greatest attraction, is represented in blue. MEP's green color refers to zero potential. According to the result of our calculation, negative potential regions are found over the copper(II) chloride group and O_{34}, while positive potential regions are found over hydrogen atoms and 1,10-Phenanthroline molecule in the MEP. In addition, the yellow color represents a lower negative potential, which can be seen above the C_9 and O_7 atoms.

Charge distributions of donor and acceptor atoms were evaluated by Mulliken atomic charges in the gas phase.

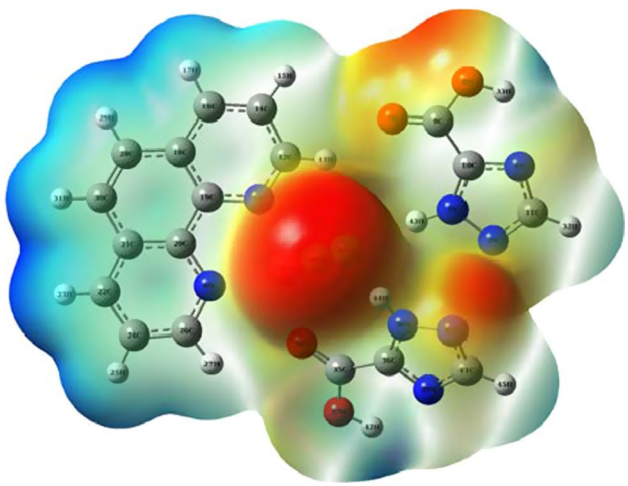

Fig. 3 Molecular electrostatic potential surface (MEP) for [Cu(phen)$(TCA)_2Cl_2$]

Cu(II) ion has a positive charge of 0.288. The charges of the nitrogen atoms of the phen ligand have similar charges − 0.236, whereas the oxygen atom of the carbonyl group is − 0.305 and two Cl anions have charges − 0.407 and − 0.411, respectively.

Fukui function

The electrophilic/nucleophilic power of an atomic site in a molecular system is determined by Fukui functions (Singha et al. 2020). Nucleophilic, electrophilic, and radical attack are expressed as f_j^+, f_j^-, and f_j^-, respectively. They are defined as follows (Mi et al. 2015):

$$f_j^+ = q_k(N+1) - q_k(N) \text{for nucleophilic attack}$$

$$f_j^- = q_k(N) - q_k(N-1) \text{for electrophilic attack}$$

$$f_j^0 = (1/2)[q_k(N+1) - q_k(N-1)] \text{for neutral (radical) attack}$$

where q_k is the atomic charge at the kth atomic site within a molecule in its neutral (N), anionic (N + 1), or cationic (N − 1) state (Saha et al. 2015). Furthermore, one of the more accurate ways to predict the electrophilic and nucleophilic susceptibility is to use the dual descriptor. It has been introduced via the following equation (Morell et al. 2005):

$$\Delta f(r) = f^+(\vec{r}) - f^-(\vec{r})$$

The site is favored for a nucleophilic attack, whereas dual descriptor $\Delta F(r) > 0$, and the site is favored for an electrophilic attack, whereas dual descriptor $\Delta F(r) < 0$. Dual descriptor and condensed Fukui functions values are reported in Supplementary Table S5. The table shows the findings of the analysis that the Cl and Cu atoms are prone to nucleophilic attack because $\Delta f(r) > 0$, while nitrogen atom (N_3) and O_7 atoms are prone to electrophilic attack because $\Delta f(r) < 0$. As a result of the calculations, f^- value of copper(II) chloride group was observed to have maximum values. Fukui functions calculations emphasize donor–acceptor interactions with other chemical species. The electrophilic and nucleophilic regions combine to provide favorable reactive sites for hydrogen-bonding interactions with selected proteins.

Frontier molecular orbital analysis and global reactivity descriptors

Frontier molecular orbitals (FMOs) electronic densities show the different types of reactions, such as conjugate structures and the most responsive state of π-electronic systems that function independently as electron donor and acceptor (Amalanathan et al. 2010). Figure 4 shows the

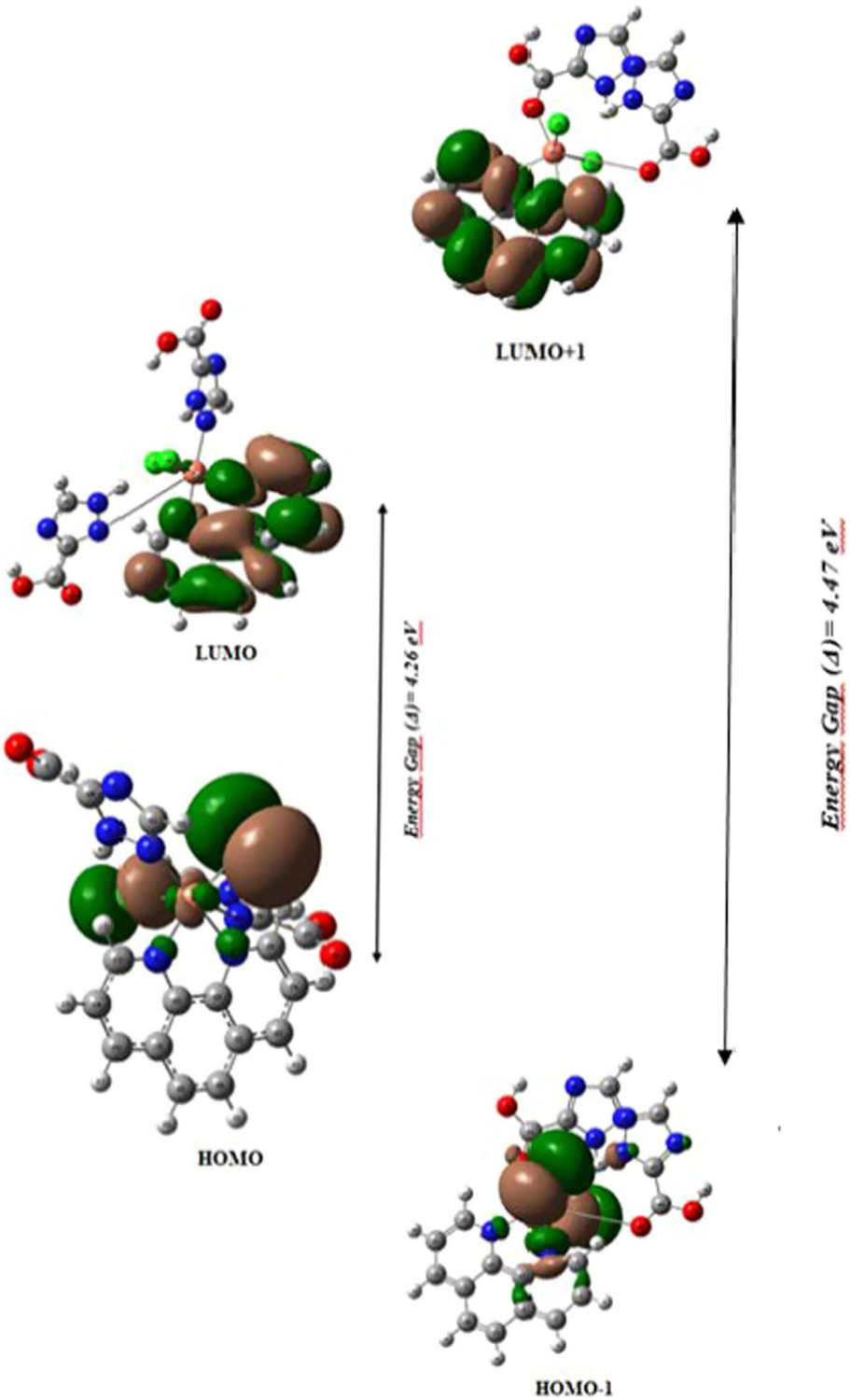

Fig. 4 Frontier molecular orbitals of $[Cu(phen)(TCA)_2Cl_2]$

spatial plots of HOMO-1, HOMO, LUMO, and LUMO + 1, as well as the energy differences of the current complex. The HOMO is localized on copper (II) transition metal and chloride ions, while the LUMO is localized over 1,10-phenanthroline molecule.

The HOMO–LUMO energy values are used to calculate global chemical reactivity parameters such as Ionization potential (*I*), electron affinity (*A*), chemical potential (μ_c), chemical hardness (η), chemical softness (σ), and electrophilicity index (ω). These parameters, which are mentioned

in Table 2, are critical in determining the chemical stability and biological activation of a system. The electrophilicity index of a molecule indicates how well a compound binds to biomolecules (Alyar and Tülin 2019; Mondal et al. 2015; Banuppriya et al. 2018). The HOMO–LUMO energy gap ($\Delta E = E_{LUMO} - E_{HOMO}$) is 4.26 eV, indicating that it makes the complex stable and can be linked with the Cu(II) complex's band gap. Moreover, this small energy difference may be interpreted as a more reactive molecule. The high electrophilicity index value (5.61 eV) of the molecule indicates that it has a higher binding capacity with biomolecules and can function as an electrophilic species, which enhances the biological activity of the molecule. While the hardness value (η) of the studied complex is 2.7097 eV, since the softness value (σ) is much smaller than this value, it shows that the Cu(II) compound can be classified as a hard material.

Wavefunctional studies

Reduced density gradient (RDG)

Reduced density gradient research visualizes the regions of a molecule where intra- and inter-non-covalent interactions happen graphically, hence playing a vital role in nature (Saleh et al. 2012). A weak association between the molecules was identified by the RDG study. The RDG can be calculated using the following equation:

$$\mathrm{RDG}(r) = 1/2\left(3\pi r^2\right)^{1/3} + |\nabla\rho(r)|/\rho(r)^{4/3}$$

where ρ(*r*) is the electron density and ∇ρ(*r*) is the gradient of ρ(*r*) at the point *r*. The graphical representation of ρ(*r*) versus sign(λ_2)ρ, where sign(λ_2)ρ is the second eigenvalue of the electron density, provides useful information regarding the strength and nature of the interactions. To comprehend the nature of inter- or intra-molecular interaction of compounds, RDG analyses have been performed and the graphs are shown in Fig. 5. According to the figure, the red region indicates strong repulsive interactions mainly observed in the copper (II) chloride group (steric effect), the blue region indicates strong attractive interactions corresponding to the strong hydrogen bonds N–H…Cl, and the green region can be identified as intermediate interactions or VdW weak attractive interactions due to H…H interaction. The regions of interactions corresponding to the hydrogen bond have a very high density of structure. The properties of electron density are dependent on these interactions.

Electron localization function (ELF)

Analysis of the electron localization function (ELF research) is used to further describe and pinpoint the chemical composition of molecules (Noureddine et al. 2020). We plotted

Table 2 The calculated HOMO–LUMO energy gaps and quantum chemical properties of title compound at DFT/LANL2DZ

No	Molecular Orbitals	Energy (eV)		Energy gap (eV)	Ionization potential (I) (eV)	Electron affinity (A) (eV)	Global hardness (η) (eV)	Electronegativity (χ) (eV)	Chemical potential (μ_c) (eV)	Global softness (σ) $(eV)^{-1}$	Electrophilicity index (ω) (eV)
1	H	− 7.02	ΔE_{H-L}	4.26	7.02	2.76	2.13	4.89	− 4.89	0.23	5.61
	L	− 2.76									
2	H − 1	− 7.10	$\Delta E_{H_{-1}-L_{+1}}$	4.47	7.10	2.62	2.24	4.86	− 4.86	0.22	5.27
	L + 1	− 2.62									
3	H − 2	− 7.16	$\Delta E_{H_{-2}-L_{+2}}$	4.88	7.16	2.28	2.44	4.72	− 4.72	0.20	4.56
	L + 2	− 2.28									

H homo, *L* lumo

$\eta = \frac{(I-A)}{2}, \mu = \frac{-(I+A)}{2}, \chi = \frac{(I+A)}{2}, \sigma = \frac{1}{2\eta}, \omega = \mu^2/2\eta$

$I = -E_{HOMO}, A = -E_{LUMO}$

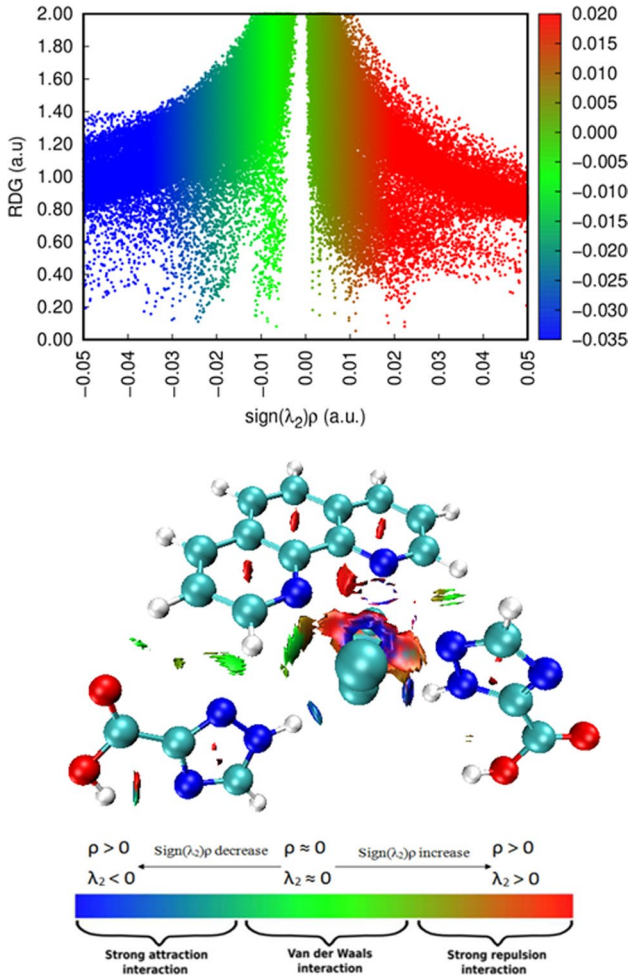

Fig. 5 2D scatter and isosurface density plots illustrating the non-bonded interactions of $[Cu(phen)(TCA)_2Cl_2]$

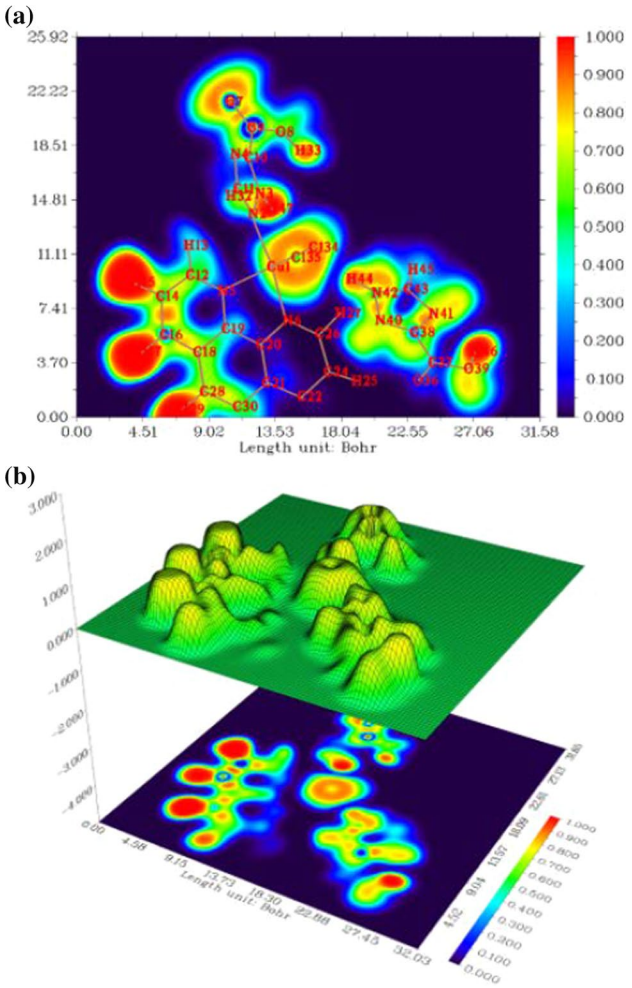

Fig. 6 Color-filled map (**a**), 3D surface-shaded projection map (**b**) of electron localization function (ELF) of $[Cu(phen)(TCA)_2Cl_2]$

the color-filled ELF map for the current molecule to get details on electron localization. This graph demonstrates that electron localization of electrons is restricted in regions of intermolecular interaction. In addition, a high ELF value results in a higher electronic position. Figure 6a shows the highly localized bond and non-bond electrons around hydrogen atoms, which are shown by elevated ELF regions. The blue regions reflect the electron cloud delocalized around those carbon atoms (C9, C16, and O7); these regions illustrate chemical bonds and chemically significant locations. The ELF map specifically shows the critical points and their courses, chemical bonds, and chemically important areas (red) (H15, H17, H29, H46). The regions surrounding hydrogen atoms have relatively high values, which indicate the binding and non-binding localized electrons. The blue circle around the C14 and C38 carbon atoms is the area where the inner layer and valence are electronically depleted.

The atoms in the highly electronic environment of the title molecule are projected by a 3D shaded surface projection diagram, as shown in Fig. 6b for the complex.

Molecular docking analysis

Molecular docking is a powerful computational tool in predicting the binding affinity of a ligand with proteins, which is useful in modern structure-based drug design. Copper complexes have indeed demonstrated a wide range of pharmacological activities such as antibacterial, antifungal antiviral, anticancer, and anti-inflammatory activity. It was found that copper complexes often demonstrate enhanced biological activity than the parent ligand alone (Chandraleka et al. 2014). 1,10-Phenanthroline metal complexes can be bacteriostatic or bactericidal toward many bacteria. Also, the compounds of the 1,2,4-triazole-3-carboxylic acid derivatives are useful in therapy, in particular for the treatment of neurological, psychiatric, pain, and gastrointestinal disorders

(Yurdakul and Tanrıbuyurdu 2012). In terms of content, the title Cu(II) complex is an interesting target for drug design. Because of the biological and pharmacological activity of the structures in the complex, various target proteins were chosen for molecular docking studies. Two different proteins were selected for mitochondrial outer membrane-anchored monoamine oxidase (MAO) and Bacillus subtilis.

The mitochondrial outer membrane-anchored monoamine oxidase (MAO) inhibitions are considered important targets for the treatment of depression, anxiety, and neurodegenerative disorders, including Alzheimer's and Parkinson's diseases (Son et al. 2008; Dhiman et al. 2019). MAO-A (PDB ID: 2Z5X) preferentially deaminates noradrenaline and serotonin. MAO-A found in the extraneuronal compartment and inside the dopaminergic, serotonergic, and noradrenergic nerve terminals (Dhiman et al. 2019). The protein–ligand interaction is found with the second chosen antibacterial receptor protein in the gram-positive bacteria Bacillus subtilis (PDB ID: 3EU4).

The bonded residues, hydrogen bonds, estimated inhibition constant, binding energy, and RMSD values of selected protein receptors can be effectively predicted using the molecular docking analysis in Table 3. While the inhibition constant due to protein–ligand interaction was determined to be smaller in the human MAO-A inhibitors, the binding energies were nearly identical. The inhibition constant is also a measure of the ligand's protein binding affinity. In general, high-affinity ligand binding provides more intermolecular strength between the ligand and its receptor, while low-affinity ligand binding has less intermolecular force. The chance of a chemical reaction between the ion and the receptor antigen increases as the Ki concentration decreases (Aycan et al. 2020). Typically, a lower Ki value indicates tighter enzyme binding and a more effective inhibitor. In other words, the smaller the inhibition constant, the fewer drugs are needed to inhibit enzyme activity (Sayin et al. 2018). As a result, our findings indicate that the 2Z5X protein could be a strong candidate for title complex inhibitors. Because the complex molecule has a low binding energy for certain proteins, it has the best binding affinity and pharmacological activity against them.

Figure 7 shows the 2D and 3D visuals of the inter-molecular interactions of the compound docked into macromolecules. Also, as shown in Table 4, in the binding site, the copper (II) complex interacted with enzymes by H-binding, π-cation and hydrophobic interactions. The 3EU4 protein-bound residue ALA191 was observed with shortest hydrogen-bonding interaction bond length of 1.81 Å, while the bonded residues of 2Z5X protein, such as HIS187, were observed with the shortest hydrogen interaction bond length of 2.02 Å. The π-cation interaction was formed between delocalized pi-electrons of the triazole ring of the complex and the residue TRY175 of the macromolecule 2Z5X (Fig. 7). Furthermore, hydrophobic interactions have been found between the Cu(II) complex's phenanthroline rings and the target proteins. These interactions are five residues of 2Z5X (LEU176, GLU327, ARG356, LYS357), while 3EU4 protein is the PHE205 amino acid residues in docking sites.

The nitrogen atoms in TCA ligand's triazole ring and oxygen in the carbonyl (C=O) group are involved as electron acceptors in target proteins (2Z5X and 3EU4). According to these observations, the copper(II) complex promotes inhibition of enzyme activity, which suggests it contributes substantially and efficiently to the treatment of antibacterial, antidepressant, and anti-anxiety disorders.

The Ramachandran plot provides essential information for determining, predicting, and validating protein structures (Anuradha et al. 2020). This indicates that most of the residues lie in the allowed region of the structure and thus may be suitable for molecular docking studies. In Fig. 8, Ramachandran plot of the two proteins is given.

Prediction of ADME parameters and toxicity

Since the toxicity of metallo-drugs is a concern, it has been suggested that drugs dependent on basic metals could be less dangerous, which has contributed to the investigation of copper-based drugs (Khodja and Boulebd 2021). The synthesized complexes were screened in this study using in silico Pre-ADMET software (www.preadmet.com.) and SwissADME (www.swissadme.ch/index.php.) to estimate their overall ADME properties and toxicity hazards, as they play an important role in drug discovery and environmental riskiness. This prediction gives results of the title compound that have shown hepatotoxicity and immunotoxicity. In this study, the result obtained for acute toxicity is in accordance

Table 3 Cu(II) complex docked against MAO-A PDB (2Z5X) and antibacterial (PDB ID: 3EU4) showing docking binding free energy (Kcal/mol), inhibition constant Ki (μM), and RMSD

Compound	Protein (PDB ID)	Binding energy (kcal/mol)	Inhibition constant K_i (μM)	Reference RMSD (Å)
[Cu(phen)$(TCA)_2$Cl2]	2Z5X	− 8.85	328.15	39.16
	3EU4	− 8.24	912.07	51.91

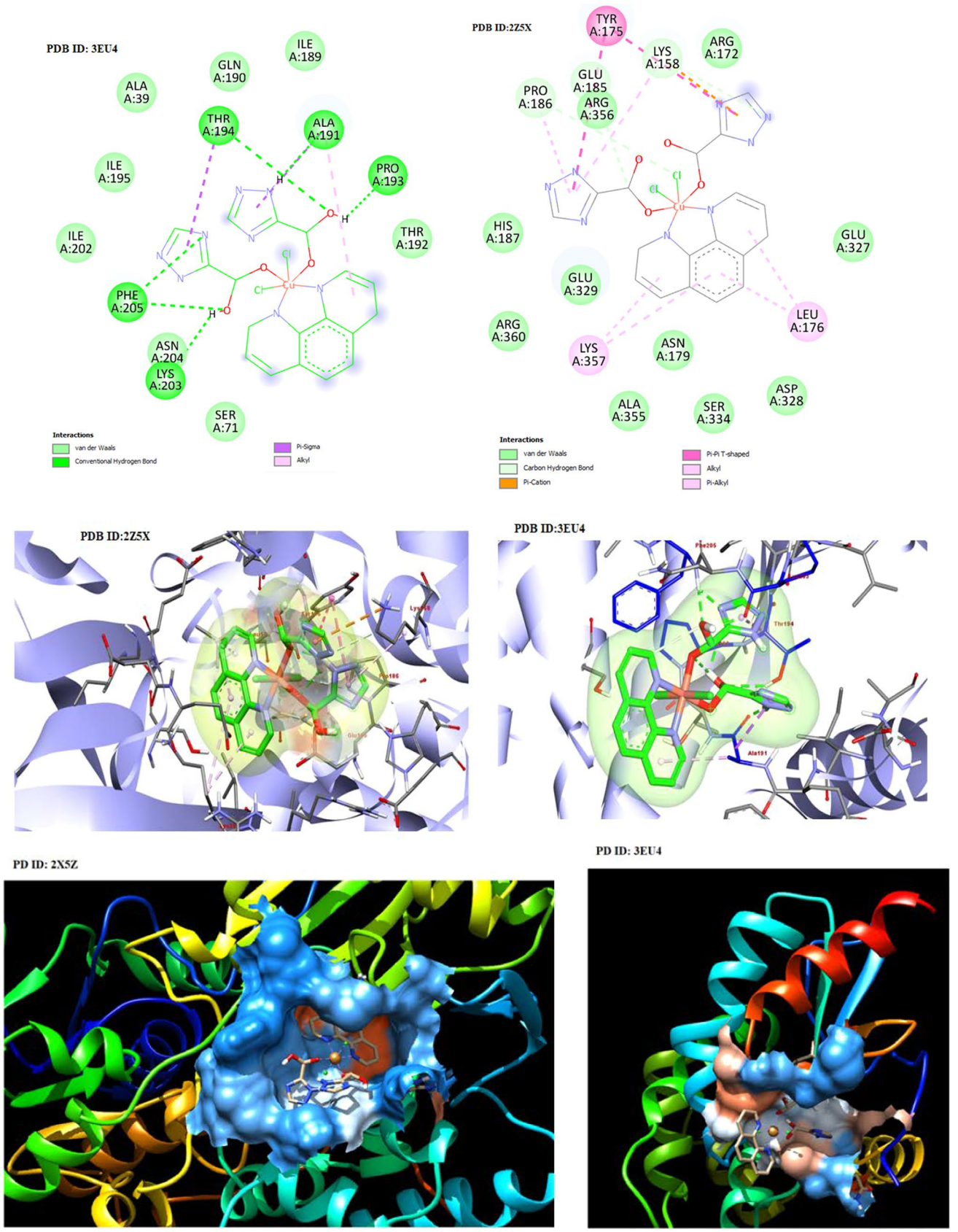

Fig. 7 Molecular docking of complex into the active site and the hydrophobic surface model of the complex with Z25X and 3EU4 proteins

Table 4 Protein–ligand interaction parameters with hydrophobic contacts for Cu(II) complex

Compound	Protein (PDB ID)	Hydrogen-bonding interaction		Hydrophobic interaction		π-Cation Interaction	
		Residues	Distance (Å)	Residues	Distance (Å)	Residues	Distance (Å)
[Cu(phen) $(TCA)_2Cl_2$]	2Z5X	ARG172	3.68	LEU176	3.40	TRY175	4.84
		HIS187	2.96	LEU176	3.19		
		HIS187	2.02	GLU327	3.81		
				ARG356	3.90		
				LYS357	2.81		
	3EU4	ALA191	1.81	PHE205	3.89		
		PRO193	1.82				
		THR194	3.01				
		ILE195	2.76				
		LYS203	1.93				
		PHE205	2.25				

with the result obtained by ProTox-II software (prediction accuracy: 12%) (Table 5).

Blood–brain barrier (BBB) penetration is used to minimize side effects and toxicity, as well as to improve the efficacy of medications with pharmacological effects on the brain. Based on its entrance into the central nervous system, the permissible range of BBB penetration for an optimal drug candidate is 0.73–0.91 (Belkhir-Talbi et al. 2019), indicating that this molecule is 0.048 outside of the acceptable range. The skin permeability, Kp, values of molecule (− 8.14 cm/h) are within the range of inferring low skin permeability (standard range − 8.0 to − 10 cm/h) (Pirhadi and Ghasemi 2012). The negative skin permeability coefficient log Kp value indicated poor skin permeability, resulting in good oral absorption. In the event of accidental contact with skin, no effect will be observed. Plasma protein binding (PPB) influences how long a drug remains in the body and may also affect its efficacy. The degree of binding to plasma proteins has a significant impact on a drug's pharmacodynamic and pharmacokinetic conduct (less than 90%). P-glycoprotein (P-gp) is one of the key threats to proper drug delivery and is in charge of extruding toxins and xenobiotics from cells. The SwissADME computed results revealed that the compound was non-inhibiting nature. The findings of human intestine absorption (HIA) value indicate that Cu(II) complex could be absorbed from the intestine into the bloodstream by 97.53%.

The ProTox-II webserver (http://tox.charite.de/protox_II/) was used to estimate the organ toxicities and toxicological end points of ligands and their LD50. In Table 6, acute toxicity estimation findings, such as LD50 value and toxicity class classifications 1 (toxic) to 6 (non-toxic), showed that the complex had no acute toxicity with a toxicity class classification of 4 (harmful if swallowed). Toxicological predictions indicate that the title copper complex was non-carcinogenic in nature and had no effect on mutagenicity and cytotoxicity. Its hepatotoxicity and immunotoxicity were active.

Antibacterial activity

The antibacterial activity of bacteria against microorganisms was studied with Cu(phen)$(TCA)_2Cl_2$. This was accomplished by disk diffusion method and minimal inhibitory concentration (MIC) on *Bacillus subtilis* bacteria using sterile media such as Mueller–Hinton agar. As a result, the *B. subtilis* zone diameter was determined as 25 mm and the MIC value was determined as 1/128.

It was used to evaluate the antibacterial properties of title copper complex against *Bacillus subtilis*. Ten mg/ml copper complex showed DIZ = 25 mm antibacterial activity with *B. subtilis.*

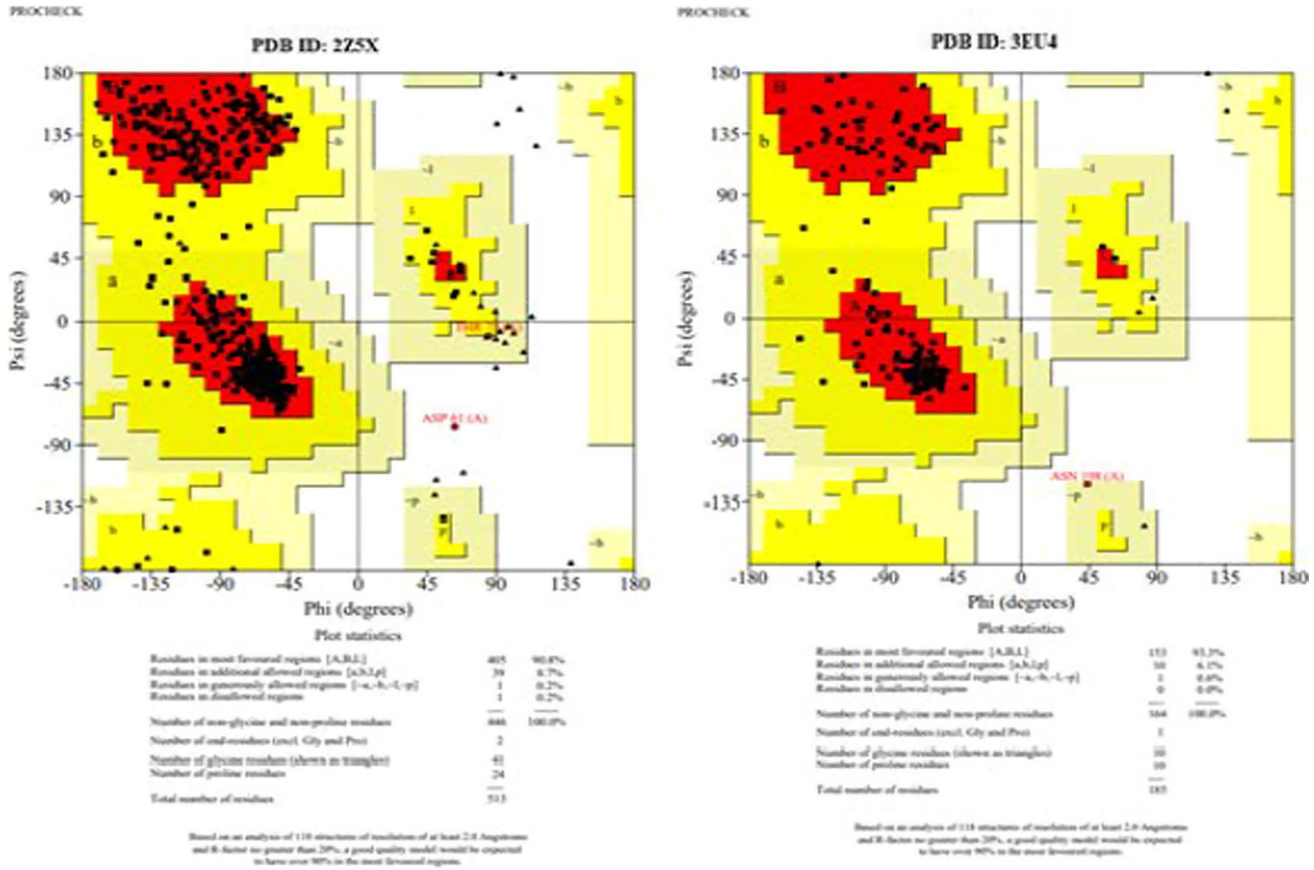

Fig.8 Ramachandran plot for 2Z5X and 3EU4

Table 5 ADME predictions of Cu(II) complex, computed by SwissADME and PreADMET

Compound	GI absorption	BBB	Caco2 permeability	HIA	Bioavailability Score	Log Kp	PPB
$[Cu(phen)(TCA)_2Cl_2]$	Low	No	1.16		97.53 0.17	− 8.14	77.40

Log Kp skin permeation value, *GI* gastrointestinal, *BBB* blood–brain barrier, *PPB* Plasma protein binding, *HIA* Human Intestinal Absorption

Table 6 Toxicity predictions of Cu(II) complex calculated by ProTox-II

Compound	Toxicity class	LD_{50} (mg/kg)	Organ toxicity			
		Hepatotoxicity	Carcinogenicity	Immunotoxicity	Mutagenicity	Cytotoxicity
$[Cu(phen)(TCA)_2Cl_2]$	4	750	Active	Inactive	Active	Inactive Inactive

Copper and its salts are traditionally well-known antimicrobial materials. These metals are believed to react with proteins by joining the –SH groups of enzymes; as a result, this reaction leads to inactivation of enzymes (Jeon et al. 2003).

Since copper and its derivatives have large specific surface areas, they are expected to show better antimicrobial properties (Sondi and Salopek-Sondi 2004).

B. subtilis, in addition to being isolated from postoperative patient wounds, causes infection in people with a very high number of microorganisms and a very low immune status. These infections include bacteremia, endocarditis, pneumonia, and septicemia (Clemente, et al. 2016; Ako-Nai et al. 2013).

Conclusion

The current study characterizes a newly synthesized copper(II) complex [Cu(phen)$(TCA)_2Cl_2$] using elemental analysis (C, H, N), FTIR, and NMR spectra. The structure of the complex was studied experimentally and theoretically. The findings achieved experimentally are quite similar to those obtained theoretically. The DFT/B3LYP/LANL2DZ level of theory was used to calculate the optimized geometry, vibrational, NBO, and chemical reactivity analyses of the title compound. Also, this work establishes a theoretical foundation for forecasting the toxicity and ADMET features of the title copper(II) complex. The molecular docking analysis performed by the monoamine oxidase (MAO) inhibitor at the active site of the human MAO-A protein (PDB ID: 2Z5X) reveals a binding energy of − 8.85 kcal/mol. A binding mode study of molecular recognition mechanisms is available to aid in the development of future selective and reversible MAO inhibitors. Our findings on [Cu(phen)$(TCA)_2Cl_2$] complex indicate that this compound has the potential to be an effective inhibitor of Parkinson's and Alzheimer's diseases. Moreover, molecular docking investigations have revealed that the complex binds to the antibacterial receptor protein gram-positive bacteria Bacillus subtilis by H-bond interactions. This indicates that the compound might be used as an antibacterial pharmacological component agent. In conclusion, Cu(phen)$(TCA)_2Cl_2$ was defined and used to evaluate the antibacterial properties of this Cu(II) complex against *B. subtilis.* Susceptibility constants were determined from the experimental results, and *B. subtilis* showed higher sensitivity to title complex. Infection after surgical intervention is an important cause of morbidity and mortality in humans. Therefore, title compound can be used as an antibacterial agent for *B. subtilis* and other bacteria responsible for postoperative wound infections. The antibacterial receptor protein Bacillus subtilis docking results showed good correlation with experimental data.

Supplementary Information The online version contains supplementary material available at https://doi.org/10.1007/s11696-022-02158-4.

Acknowledgements The authors are thankful to Belgin ERDEM (Kırşehir Ahi Evran University) for the antibacterial activity part of the manuscript.

Authors' contributions Material preparation, data collection, and analysis were performed by SC, SB, and ŞY. The software and formal analysis was performed by SC. Writing—review and editing of the manuscript was done by SC, SB, and ŞY. All authors commented on previous versions of the manuscript. All authors contributed to the study conception and design and approved the final manuscript.

Funding This research received no external funding.

Availability of data and material The article files will be available upon request.

Code availability The calculations have been carried out using Gaussian09 and Gauss view version provided by Gaussian Inc.

Declarations

Conflict of interest The authors declare that they have no known competing financial interests or personal relationships that could have appeared to influence the work reported in this paper.

References

Accorsi G, Listorti A, Yoosaf K, Armaroli N (2009) 1, 10-phenanthrolines: versatile building blocks for luminescent molecules, materials and metal complexes. Chem Soc Rev 38:1690–1700

Ajayi TJ, Shapi M (2020) Solvent-free mechanochemical synthesis, Hirshfeld surface analysis, crystal structure, spectroscopic characterization and NBO analysis of Bis(ammonium) Bis((4-methoxyphenyl) phosphonodithioato)-nickel (II) dihydrate with DFT studies. J Mol Struct 1202:127254

Ako-Nai AK, Abumere G, Akinyoola AL, OT, Kassim OO, (2013) Characterization of bacterial isolates from patients wounds and environmental factors predictive of post-surgical infections at the orthopedic ward in ile-ife. Nigeria East Afr Med J 90(12):380–386

Alyar S, Tülin S (2019) Synthesis, spectroscopic characterizations, enzyme inhibition, molecular docking study and DFT calculations of new Schiff bases of sulfa drugs. J Mol Struct 1185:416–424

Amalanathan M, Joe IH, Prabhu SS (2010) Charge transfer interaction and terahertz studies of a nonlinear optical material glutamine picrate: a DFT study. J Phys Chem A 114:13055–13064

Anuradha A, Sara Saji R, Varghese MG, Muthu S, Prasana JC (2020) Vibrational spectroscopic, DFT studies and molecular docking on (2R)-2-acetamido-N-benzyl-3-methoxy propanamide as an antineuropathic pain drug. Mater Today

Aycan T, Öztürk F, Doruk T, Demir S, Fidan M, Paşaoğlu H (2020) Synthesis, structural, spectral and antimicrobial activity studies of copper-nalidixic acid complex with 1,10-phenanthroline: DFT and molecular docking. Spectrochim Acta Part A Mol Biomol Spect 241:118639

Balci M (2005) Basic 1H- and 13C-NMR spectroscopy. Elsevier, Amsterdam. ISBN: 9780444518118

Banuppriya G, Sribalan R, Padmini V (2018) Synthesis and characterization of curcumin-sulfonamide hybrids: Biological evaluation and molecular docking studies. J Mol Struct 1155:90–100

Belkhir-Talbi D, Makhloufi-Chebli M, Terrachet-Bouaziz S, Hikem-Oukacha D, Ghemmit N, Ismaili L, Silva AMS, Hamdi M (2019) Synthesis, characterization, theoretical studies, ADMET and drug-Likeness analysis: electrochemical and biological activities of metal complexes of 3-(2-hydroxybenzoyl)-2H-chromen-2-one. J Mol Struct 1179:495–505

Bencini A, Lippolis V (2010) 1, 10-Phenanthroline: a versatile building block for the construction of ligands for various purposes. Coord Chem Rev 254:2096–2180

Bergamo A, Dyson PJ, Sava G (2018) The mechanism of tumor cell death by metal based anticancer drugs is not only a matter of DNA interactions. Coord Chem Rev 360:17–33

Chandraleka S, Ramya K, Chandramohan G, Dhanasekaran D, Priyadharshini A, Panneerselvam A (2014) Antimicrobial mechanism of copper (II) 1,10-phenanthroline and 2,20 -bipyridyl complex on bacterial and fungal pathogens. J Saudi Chem Soc 18:953–962

Chen X-B, Chen B, Li Y-Z, You X-Z (2007) Remarkable solvent effects in the hydro- and solvothermal synthesis of copper-1,10-phenanthroline complexes. Appl Organometal Chem 21:777–781

Clemente L, Dragovic D, Milocco C, Fontana F (2016) Report of a rare case of sepsis caused by Bacillus pumilus in an immunocompetent child with the involvement of soft tissues cellulitis. Microbiologia Medica 31:118–119

DeLano WL (2002) Pymol: an open-source molecular graphics tool. CCP4 Newslett Prot Crystallogr 40:82–92

Dennington R, Keith T, Millam J (2009) GaussView version 5. Semichem Inc., Shawnee Mission, KS

Dhiman P, Malik N, Sobarzo-Sánchez E, Uriarte E, Khatkar A (2019) Quercetin and related chromenone derivatives as monoamine oxidase inhibitors: targeting neurological and mental disorders. Molecules 24:418–436

Dunaj-Jurco M, Ondrejovic G, Melnik M, Garaj J (1988) Mixed-valence copper(I)-copper(II) compounds: analysis and classification of crystallographic data. Coord Chem Rev 83:1–28

Erdogdu Y, Başköse ÜC, Sağlam S (2019) Conformational, structural, electronic, and vibrational investigations on 5-methyl-4-(2-thiazolylazo)resorcinol by FT-IR, FT–Raman, NMR, and DFT. Chem Pap 73:1879–1891

Frisch MJ, Trucks GW, Schlegel HB, Scuseria GE, Robb MA, Cheeseman JR, Scalmani G, Barone V, Mennucci B, Petersson GA, Nakatsuji H, Caricato M, Li X, Hratchian HP, Izmaylov AF, Bloino J, Zheng G, Sonnenberg JL, Hada M, Ehara M, Toyota K, Fukuda R, Hasegawa J, Ishida M, Nakajima T, Honda Y, Kitao O, Nakai H, Vreven T, Montgomery JA Jr, Peralta JE, Ogliaro F, Bearpark M, Heyd JJ, Brothers E, Kudin KN, Staroverov VN, Kobayashi R, Normand J, Raghavachari K, Rendell A, Burant JC, Iyengar SS, Tomasi J, Cossi M, Rega N, Millam JM, Klene M, Knox JE, Cross JB, Bakken V, Adamo C, Jaramillo J, Gomperts R, Stratmann RE, Yazyev O, Austin AJ, Cammi R, Pomelli C, Ochterski JW, Martin RL, Morokuma K, Zakrzewski VG, Voth GA, Salvador P, Dannenberg JJ, Dapprich S, Daniels AD, Farkas O, Foresman JB, Ortiz JV, Cioslowski J, Fox DJ (2009) Gaussian, Inc., Wallingford CT

Hammuda HH, Kortz U, Bhattacharya S, Demirdjian S, Haririd E, Isbere S, Sang E, Choi ES, Mirtamizdoustg B, Mrouehh M, Daher CF (2020) Structure, DFT studies, magnetism and biological activity of bis[(μ-azido)-chloro-(1,10-phenanthroline)-copper(II)] complex. Inorg Chim Acta 506:119533

Henkel G, Weissgräber S, Buse G, Soulimane T, Steffens GCM, Nolting H-F (1995) The active sites of the native cytochrome-c oxidase from bovine heart mitochondria: EXAFS-spectroscopic characterization of a novel homobinuclear copper center (CuA) and of the heterobinuclear Fea3-CuB center. Angew Chem Int Edn Engl 34:1488–1492

Houser RP, Young VG, Tolman WB (1996) A thiolate-bridged, fully delocalized mixed-valence dicopper (I, II) complex that models the Cu A biological electron-transfer site. J Am Chem Soc 118:2101–2102

Humphrey W, Dalke A, Schulten K (1996) VMD: visual molecular dynamics. J Mol Graph 14:33–38

Jeon HJ, Yi SC, Oh SG (2003) Preparation and antibacterial effects of AgSiO2 thin films by sol-gel method. Biomaterials 24:4921–4928

Kargar H, Behjatmanesh-Ardakani R, Torabi V, Kashani M, Chavoshpour-Natanzi Z, Kazemi Z, Mirkhani V, Sahraei A, Nawaz Tahir M, Ashfaq M, Munawar KS (2021a) Synthesis, characterization, crystal structures, DFT, TD-DFT, molecular docking and DNA binding studies of novel copper(II) and zinc(II) complexes bearing halogenated bidentate N,O-donor Schiff base ligands. Polyhedron 195:114988

Kargar H, Behjatmanesh-Ardakani R, Torabi V, Sarvian A, Kazemi Z, Chavoshpour-Natanzi Z, Mirkhani V, Sahraei A, Tahir MN, Ashfaq M (2021b) Novel copper(II) and zinc(II) complexes of halogenated bidentate N,O-donor Schiff base ligands: Synthesis, characterization, crystal structures, DNA binding, molecular docking, DFT and TD-DFT computational studies. Inorg Chim Acta 14:120004

Kargar H, Aghaei-Meybodi F , Behjatmanesh-Ardakani R, Reza Elahifard M, Torabi V, Fallah-Mehrjardi M, Nawaz Tahir M, Ashfaq M, Munawar KS (2021c) Synthesis, crystal structure, theoretical calculation, spectroscopic and antibacterial activity studies of copper(II) complexes bearing bidentate schiff base ligands derived from 4-aminoantipyrine: influence of substitutions on antibacterial activity. J Mol Struct 1230:129908

Khodja IA, Boulebd H (2021) Synthesis, biological evaluation, theoretical investigations, docking study and ADME parameters of some 1,4-bisphenylhydrazone derivatives as potent antioxidant agents and acetylcholinesterase inhibitors. Mol Divers 25:279–290

Lappalainen P, Saraste M (1994) The binuclear CuA center of cytochrome oxidase. Biochim Biophys Acta 1187:222–225

Liu J-n, Chen Z-r, Yuan S-f (2005) Study on the prediction of visible absorption maxima of azobenzene compounds. J Zhejiang Univ Sci B 6:584–589

Lu T, Chen F (2012) Multiwfn: a multifunctional wavefunction analyzer. J Comput Chem 33:580–592

Luman CR, Castellano FN (2003) Phenanthroline Ligands Compr Coord Chem II:25–39

Machura B, Wolff M, Jaworska M, Lodowski P, Benoist E, Carrayon C, Saffon N, Kruszynski R, Mazurak Z (2011) Rhenium(I) carbonyl complex of 4,7-diphenyl 1,10-phenanthrolineeSpectroscopic properties, X-ray structure, theoretical studies of ground and excited electronic states. J Organomet Chem 696:3068–3075

Malmatrom BG, Aasa R (1993) The nature of the Cu Acenter in cytochrome coxidase. FEBS Lett 325:49–52

Mi H, Xiao G, Chen X (2015) Theoretical evaluation of corrosion inhibition performance of three antipyrine compounds. Comp Theor Chem 1072:7–14

Mondal S, Mandal SM, Mondal TK, Sinha C (2015) Structural characterization of new Schiff bases of sulfamethoxazole and sulfathiazole, their antibacterial activity and docking computation with DHPS protein structure. Spectrochim Acta A Mol Biomol Spectrosc 150:268–279

Morell C, Grand A, Toro-Labbe A (2005) New dual descriptor for chemical reactivity. J Phys Chem 109:205–212

Morris GM, Goodwill DS, Halliday RS, Huey R, Hart W, Belew RK, Olson AJ (1998) Automated docking using a Lamarckian genetic algorithm and an empirical binding free energy function. J Comp Chem 19:1639–1662

Noureddine O, Gatfaoui S, Brandan SA, Sagaama A, Marouani H, Issaoui N (2020) Experimental and DFT studies on the molecular structure, spectroscopic properties, and molecular docking of 4-phenylpiperazine-1-ium dihydrogen phosphate. J Mol Struct 207:127762

Onawumi OOE, Adeoye IO, Adekunle FAO (2013) Synthesis, characterization and microbial studies of [bis(1,10-phenanthroline) (ethylenediamine) copper(II)] diperchlorate and its bromide analogue. Open J Inorg Chem 3:26–33

Osmialowski B, Kolehmainen E, Gawinecki E (2001) GIAO/DFT calculated chemical shifts of tautomeric species. 2-Phenacylpyridines and (Z)-2-(2-hydroxy-2-phenylvinyl)pyridines. Magn Res Chem 39:334–340

Pirhadi S, Ghasemi JB (2012) Pharmacophore identification, molecular docking, virtual screening, and in silico ADME studies of non-nucleoside reverse transcriptase inhibitors. Mol Inf 31:856–866

Pophristic V, Goodman L, Guchhait N (1997) Role of lone-pairs in internal rotation barriers. J Phys Chem 101:4290–4297

Ramakrishnan S, Palaniandavar M (2005) Mixed-ligand copper(II) complexes of dipicolylamine and 1,10-phenanthrolines: the role

of diimines in the interaction of the complexes with DNA. J Chem Sci 117:179–186
Reiher M, Brehm G, Schneider S (2004) Assignment of vibrational spectra of 1,10-phenanthroline by comparison with frequencies and Raman intensities from density functional calculations. J Phys Chem A 108:734–742
Robertazzi A, Vittorio Vargiu A, Magistrato A, Ruggerone P, Carloni P, de Hoog P, Reedijk J (2009) Copper-1,10-phenanthroline complexes binding to DNA: structural predictions from molecular simulations. J Phys Chem B 113:10881–10890
RSCB PDB Protein Data Bank (2021) https://www.rcsb.org/. Accessed 01 October 2021
Saha SK, Ghosh P, Hens A, Murmu NC, Banerjee P (2015) Density functional theory and molecular dynamics simulation study on corrosion inhibition performance of mild steel by mercapto-quinoline Schiff base corrosion inhibitor. Phys E Low-Dimens Syst Nanostruct 66:332–341
Saleh G, Gatti C, Lo Presti L (2012) Non-covalent interaction *via* the reduced density gradient: independent atom model *vs* experimental multipolar electron densities. Comp Theo Chem 998:148–163
Sayin K, Karakaş D, Kariper SE, Sayin TA (2018) Computational study of some fluoroquinolones: structural, spectral and docking investigations. J Mol Struct 1156:172–181
Schilt A, Taylor RC (1959) Infra-Red spectra of 1:10-Phenanthroline metal complexes in the rock salt region below 2000 cm^{-1}. J Inorg Nucl Chem 9:211–221
Singha K, Bala I, Kataria R (2020) Crystal structure, Hirshfeld surface and DFT based NBO, NLO, ECT and MEP of benzothiazole based hydrazine. Chem Phys 538:110873
Son S-Y, Ma J, Kondou Y, Yoshimura M, Yamashita E, Tsukihara T (2008) Structure of human monoamine oxidase A at 2.2-Å resolution: the control of opening the entry for substrates/inhibitors. PNAS 105:5739–5744
Sondi I, Salopek-Sondi B (2004) Silver nanoparticles as antimicrobial agent: a case study on E. coli as a model for Gram-negative bacteria. J Colloid Interface Sci 275:177–182
Tapiero H, Townsend DM, Tew KD (2003) Trace elements in human physiology and pathology. Copper Biomed Pharmacother 57:386–398
Weinhold F (2005) Chemistry: a new twist on molecular shape. Nature 411:539–541
Yurdakul Ş, Tanrıbuyurdu S (2012) FT-IR, FT-Raman, vibrational assignments, and density functional studies of 1,2,4-triazole-3-carboxylic acid, and its tautomers, dimers. Struct Chem 23:433–440
Zhu J, Yin X-H, Feng Y, Zhang S-S, Zhao K, Lin C-W (2008) Chlorido(1,10-phenanthroline)(1H-1,2,4- triazole-3-carboxylato) copper(II). Acta Cryst E64: m71